Journal of Power Sources 236 (2013) 311–320

Contents lists available at SciVerse ScienceDirect

Journal of Power Sources

journal homepage: www.elsevier.com/locate/jpowsour

Oxygen reduction activity of binary PtMn/C, ternary PtMnX/C (X = Fe, Co, Ni, Cu, Mo and, Sn) and quaternary PtMnCuX/C (X = Fe, Co, Ni, and Sn) and PtMnMoX/C (X = Fe, Co, Ni, Cu and Sn) alloy catalysts

Malika Ammam, E. Bradley Easton*

Faculty of Science, University of Ontario Institute of Technology, 2000 Simcoe Street North, Oshawa, ON L1H 7K4, Canada

HIGHLIGHTS

- ► Binary alloy PtMn/C is evaluated towards ORR.
- ► Ternary PtMnX/C (X = Fe, Co, Ni, Cu, Mo and, Sn) alloys were evaluated towards ORR.
- ► Quaternary PtMnCuX/C (X = Fe, Co, Ni, and Sn) alloys were evaluated towards ORR.
- ► Quaternary PtMnMoX/C (X = Fe, Co, Ni, Cu and Sn) alloys were evaluated towards ORR.
- ► PtMnCu/C, PtMnCuFe/C and PtMnMoCu/C were found to be the best catalysts for ORR.

ARTICLE INFO

Article history:
Received 10 December 2012
Received in revised form
2 February 2013
Accepted 11 February 2013
Available online 26 February 2013

Keywords:
O_2 reduction
Electrocatalysis
Alloy catalysts

ABSTRACT

In this study, we evaluated the activity of binary PtMn/C, ternary PtMnX/C (X = Fe, Co, Ni, Cu, Mo and, Sn) and quaternary PtMnCuX/C (X = Fe, Co, Ni, and Sn) and PtMnMoX/C (X = Fe, Co, Ni, Cu and Sn) alloy catalysts towards the oxygen reduction reaction (ORR) in acidic solution. Although all catalysts exhibited improved activities towards the ORR if normalized by the mass of Pt; when they are considered per milligram of total metal only a handful of them illustrated improved activities towards the ORR in terms of onset potential and current intensity determined by cyclic voltammetry with respect to pure Pt/C. PtMnCu/C, PtMnCuFe/C and PtMnMoCu/C were found to be the best catalysts for ORR. In order to gain a better understanding of the pathways of ORR, Pt/C, PtMnCu/C, PtMnCuFe/C and PtMnMoCu/C were further studied using a Rotating Disk Electrode (RDE) and Rotating Ring Disk Electrode (RRDE). Tafel plots and Koutecky–Levich analysis of the data revealed that the activity towards the ORR is better with PtMnMoCu/C followed by PtMnCuFe/C and PtMnCu/C. The estimated average number of the electrons transferred during the ORR process was found to be around $4e^-$. The average percentage of the generated H_2O_2 reached as high as ~7.5% with PtMnMoCu/C. All these data point to the fact that the pathways of ORR which produce H_2O_2 and H_2O as final products took place. As a final comparison for this series of catalysts, this study also gives a better selection of the catalysts that may preferably be used at the anode for ethanol oxidation or at the cathode for ORR to yield fuel cells with substantial output voltages.

1. Introduction

The fuel cell is a promising alternative to environmentally unfriendly devices that are currently powered by fossil fuels [1,2]. There are various kinds of fuel cells such as polymer electrolyte membrane fuel cell, phosphoric acid fuel cell, alkaline fuel cell, solid oxide fuel cell and direct alcohol fuel cell. Among these, direct alcohol fuel cells (DAFCs) are considered highly promising power devices due to advantages like: i) simplified liquid fuel storage compared to hydrogen gas storage, ii) low operating temperatures and, iii) easy handling. On the other hand, although all these fuel cells employ different fuels at the anode, all of them use oxygen fuel at the cathode [3,4].

The electrocatalytic reduction of dioxygen (O_2) at a reasonably low overpotential has been the aim of numerous studies. This reaction plays a very important role in the cathode of fuel cells. Many types of electrocatalysts for O_2 reduction have been investigated either in alkaline or acidic media [5–10]. In regard to this, oxygen reduction reaction (ORR) on noble metal surfaces such as platinum

* Corresponding author. Tel.: +1 905 721 8668x2936; fax: +1 905 721 3304.
E-mail addresses: m78ammam@yahoo.fr (M. Ammam), Brad.Easton@uoit.ca (E.B. Easton).

0378-7753/$ – see front matter © 2013 Elsevier B.V. All rights reserved.
http://dx.doi.org/10.1016/j.jpowsour.2013.02.029

(Pt) remains as one of the well-investigated electrochemical processes. However, due to kinetic limitations of the ORR, the cathodic overpotential losses amount to several hundreds of millivolts under typical operation condition of fuel cells [11]. In the last decades efforts were undertaken to optimize the catalyst towards the ORR in order to avoid voltage losses. For that, a variety of binary, ternary and even quaternary Pt alloys catalysts have been investigated for the ORR [12–20]. The results obtained throughout these studies are by no means consistent. For example, when investigating PtCr, PtV, PtCrCo and PtVCo alloys instead of pure Pt, Luczak and Landsman [21–23] found an increase in mass activity by factor of 1.5–2.5 (at 0.9 V) whereas Beard and Ross [24] and Glass et al. [25] noticed no increase in the activity of PtCo and PtCr alloys compared to Pt. As reported by Beard and Ross [24], it is generally assumed that comparison between supported alloys catalysts with respect to pure Pt is difficult. The reason for that has to do first with the metal nanoparticle composition that may promote or not the ORR. Second, the activity of supported metal nanoparticles can also depend on the particle size, shape and distribution on the supporting carbon.

We have previously reported the synthesis, characterization and activity towards ethanol oxidation of a series of binary PtMn/C, ternary PtMnX/C (X = Fe, Co, Ni, Cu, Mo and, Sn) and quaternary PtMnCuX/C (X = Fe, Co, Ni, and Sn) and PtMnMoX/C (X = Fe, Co, Ni, Cu and Sn) alloy catalysts [26–28]. Overall we demonstrated that these catalysts exhibited an enhanced activity towards ethanol oxidation. In the course of this study, we have examined the series of alloy catalysts towards the ORR under the same condition in order to identify the best catalysts that might be of interest to use in cathodes of fuel cells.

2. Experimental

2.1. Catalyst synthesis

Pt/C, PtMn (19:81)/C, PtMnX/C (X = Fe, Co, Ni, Cu, Mo and, Sn) and PtMnCuX/C (X = Fe, Co, Ni, and Sn) and PtMnMoX/C (X = Fe, Co, Ni, Cu and Sn) alloy catalysts have been synthetized as previously reported [26–28]. Briefly, for the synthesis of PtMn (19:81)/C, $H_2PtCl_6.6H_2O$ (Aldrich) and $MnCl_2.2H_2O$ (Aldrich) at the ratio of 23:77 were mixed in ultrapure water (Milli-Q, 18.2 MΩ cm). After 15 min of constant stirring Vulcan XC72R carbon black (Cabot) was added to the solution in an amount to give a total metal content of 20 wt%. PtMn nanoparticles supported on carbon were formed by reduction of the metal precursors with $NaBH_4$, which was added as a solid to the mixture in a weight ratio of 3:1 to metals. The resulting mixture was then left under constant stirring over night and the formed supported catalysts were collected via suction filtration, washed thoroughly with ultrapure water, ethanol and acetone and finally dried over night at 80 °C. The ternary alloy catalysts PtMnX/C (X = Fe, Co, Ni, Cu, Mo and, Sn) were prepared using the same procedure by replacing 20% (w/w) of $MnCl_2.2H_2O$ (Aldrich) by $FeCl_3.6H_2O$ (Gelest Inc.), $Co(NO_3)_2.6H_2O$ (Sigma–Aldrich), $NiCl_2$ (Fluka), $CuCl_2.2H_2O$ (Sigma–Aldrich), $(NH_4)_2MoO_4$ (Aldrich) or $SnCl_2$ (Aldrich). The quaternary alloys were also formed following the same procedure by replacing 10% (w/w) of $CuCl_2.2H_2O$ (Sigma–Aldrich) in PtMnCu/C by $FeCl_3.6H_2O$ (Gelest Inc.), $Co(NO_3)_2.6H_2O$ (Sigma–Aldrich), $NiCl_2$ (Fluka), or $SnCl_2$ (Aldrich) and, 10% (w/w) of $(NH_4)_2MoO_4$ in PtMnMo/C by $FeCl_3.6H_2O$ (Gelest Inc.), $Co(NO_3)_2.6H_2O$ (Sigma–Aldrich), $NiCl_2$ (Fluka), $CuCl_2.2H_2O$ (Sigma–Aldrich) or $SnCl_2$ (Aldrich).

Table 1
Summary of the synthetized catalysts, their compositions determined by ICP as well as the average grain size calculated from X-ray diffraction data using the Debye–Scherrer equation. Table summarized from Refs. [26–28].

Electrocatalysts	Molar ratios measured by ICP				Grain size (nm ± 0.5)	
	Pt	Mn	–	–	Cubic	Tetragonal
Pt/C	100	0	–	–	8.5	–
PtMn/C	19	81	–	–	7.5	–
	Pt	Mn	X	–	Cubic	Tetragonal
PtMnFe/C	18	52	30	–	3.1	–
PtMnCo/C	19	54	27	–	5.0	–
PtMnNi/C	17	48	35	–	6.0	–
PtMnCu/C	17	43	40	–	3.1	–
PtMnMo/C	17	61	22	–	4.5	–
PtMnSn/C	17	44	39	–	8.0	17.0
	Pt	Mn	Cu	X	Cubic	Tetragonal
PtMnCu/C	17	43	40		3.5	–
PtMnCuFe/C	31	40	18	11	3.1	–
PtMnCuCo/C	17	46	24	13	4.0	–
PtMnCuNi/C	26	42	20	12	4.0	–
PtMnCuSn/C	24	30	12	34	5.0	17.0
	Pt	Mn	Mo	X	Cubic	Tetragonal
PtMnMo/C	17	61	22	–	4.5	–
PtMnMoFe/C	21	41	24	14	6.0	–
PtMnMoCo/C	12	67	4	17	6.0	–
PtMnMoNi/C	30	48	6	16	6.0	–
PtMnMoCu/C	31	50	4	15	4.5	–
PtMnMoSn/C	14	37	3	46	6.0	26.0

2.2. Materials characterization

Inductively Coupled Plasma Optical Emission Spectrometry (ICP-OES) was utilized for quantitative determination of metal content in the catalysts. 5 mg of each catalyst was dissolved in nitric acid (>70%) and left to dissolve for at least 1 week. Afterwards, the solutions were filtered off to separate the supporting carbon from the solution and yield a clear solution for ICP-OES analyses. Standardization was performed with three Pt, Mn and X solutions ranging from approximately 1–20 ppm. These standards contained approximately 2% nitric acid to ensure the complete dissolution and keep both sample and standard matrices equivalent.

Transmission Electron Microscopy (TEM) images were acquired using a Philips CM10 instrument equipped with an AMT digital camera system. Catalysts powders were dispersed in ultrapure water and applied to nickel 400 mesh formvar coated carbon reinforced grids and allowed to dry under air. Grids were then scanned in a Philips CM10 TEM at 100 kV.

Table 1 gathers the list of the synthetized catalysts; their molar ratios determined by ICP and as well as the average grain size of the catalysts nanoparticles estimated from XRD [26–28].

2.3. Electrochemical characterization

The electrocatalytic activity of the catalysts towards ORR was measured through the preparation of electrode inks, which were prepared as follows: 11 mg of the synthetized electrocatalyst was dispersed in 500 μL of a mixture of ultrapure water and 2-propanol (1:1 by volume) and the suspension was stirred in an ultrasonic bath for 15 min. 5 μL of the catalysts ink was immobilized onto the surface of either a glassy carbon (GC) electrode (diameter = 3 mm, CH Instruments), rotating disk electrode (diameter = 5 mm, Pine Instruments) and a rotating ring disk electrode which is composed of a platinum ring (7.5 and 8.5 mm inside and outside diameters, respectively) surrounded the glassy carbon disk (diam = 5 mm), and dried at 80 °C for 20 min. Prior to use, the electrodes were first polished with 6, 3 and 1 μm alumina then abundantly rinsed with ultrapure water and acetone. The final loading of metal catalysts on each electrode was 0.30 ± 0.03 mg cm^{-2}.

Electrochemical measurements were performed using either a Solartron SI 1286 potentiostat controlled using Corrware software

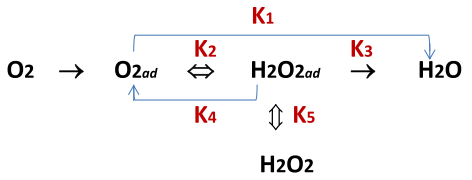

Scheme 1. Representation of the different possible pathways of the ORR as proposed by Wroblowa et al. [34].

(Scribner Associates) or a Pine Instruments AFCBP1 bipotentiostat controlled using Aftermath software. A three-compartment electrochemical cell was used. The side arms contained a Ag/AgCl 3 M KCl (0.210 V versus NHE) reference electrode and a platinum counter electrode. Measurements were made at room temperature using either N_2-purged 0.5 M H_2SO_4 (aq) or O_2 saturated 0.5 M H_2SO_4. The hydrogen peroxide detection and quantification occurred by measuring the Pt ring current. The Pt ring electrode was potentiostated at 0.99 V vs. Ag/AgCl during the measurement of the ORR polarization curve on the catalytic film disk electrode. The H_2O_2% was estimated from the following relationship [6,29–32]:

$$H_2O_2\% = \frac{200I_r}{NI_d + I_r} \quad (1)$$

where I_r is the current obtained from the ring, I_d is the current obtained from the disk, and N is the collection efficiency, which was determined as 0.1933 for our system through ferricyanide calibration.

3. Results and discussion

3.1. ORR pathway on Pt and Pt alloys catalysts

ORR is a multielectron reaction that may include a number of elementary steps involving different reaction intermediates. Among the different proposed reactions pathways of the ORR [33], the scheme suggested by Wroblowa et al. [34] appears to be the most effective one to describe the complicated reaction pathway by which O_2 is reduced at metal surfaces (Scheme 1).

Based on this reaction scheme, O_2 can be electrochemically reduced either directly to water with $4e^-$ reaction following the rate constant k_1 without intermediate formation of H_2O_{2ad} or to H_2O_{2ad} with $2e^-$ reduction reaction following the rate constant k_2. The adsorbed H_2O_2 can be electrochemically reduced to water with the rate constant k_3 with a $2e^-$ pathway, catalytically (chemically) decomposed on the electrode surface (k_4) or desorbed into the bulk of the solution (k_5). Although a number of important problems pertaining to the interpretation of the reaction pathway for the ORR on Pt have yet to be resolved, some studies [35–38] suggest that a series pathway via an $(H_2O_2)_{ad}$ intermediate may be operative on Pt and Pt bimetallic catalysts. This can be considered as a special case of the general mechanism where k_1 is essentially zero, i.e., there is no splitting of the O–O bond before H_2O_2 species is formed. H_2O_2, on the other hand may ($k_5 = 0$) or may not be further reduced to water. In either case, the rate determining step appears to be the addition of the first electron to O_{2ad}. Thermodynamically speaking, the reduction potential of O_2 into H_2O_2 presented in Scheme 1 with rate constant k_2 is lower than the potential required to form H_2O

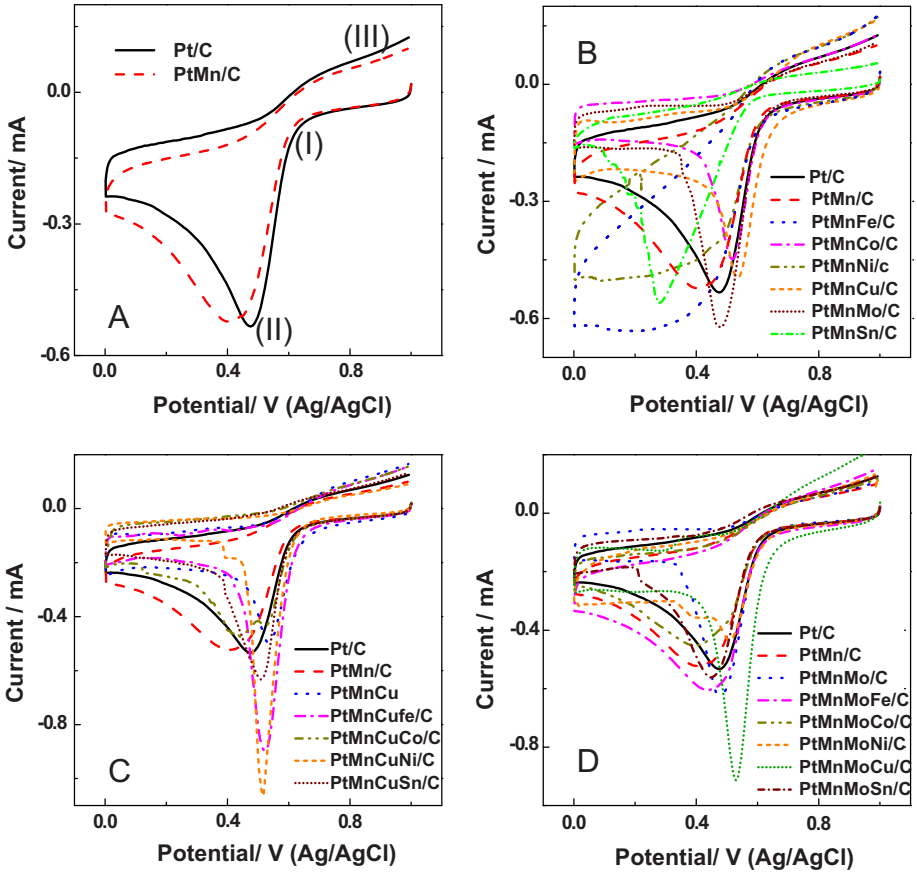

Fig. 1. Cyclic voltammetry curves of binary PtMn/C, ternary PtMnX/C (X = Fe, Co, Ni, Cu, Mo and, Sn) and quaternary PtMnCuX/C (X = Fe, Co, Ni, and Sn) and PtMnMoX/C (X = Fe, Co, Ni, Cu and Sn) alloys catalysts in 0.5 M H_2SO_4 saturated with O_2 without hydrodynamic agitation. The data were collected under similar conditions to allow a proper comparison. Scan rate 20 mV s^{-1}. (I) is the onset potential of ORR, (II) is the current intensity peak due ORR and, (III) is the oxidation peak current of H_2O_2 produced from ORR.

Table 2
Summary of the synthesized catalysts and estimate ECSA, onset potential, peak potential, current intensity of the O_2 reduction and current intensity of the H_2O_2 oxidation taken from the cyclic voltammetry curves of Fig. 1. Also is shown onset potential of the ethanol oxidation reaction (EOR) and the preference of the catalyst to be used at anode or cathode of fuel cells (ethanol/O_2) evaluated from the difference in onset potentials with respect to pure Pt/C. The onset potentials are determined at the starting catalytic currents of the O_2 reduction of ethanol oxidation or O_2 reduction obtained by overlaying the cyclic voltammograms of the catalysts in presence of O_2 or ethanol with the blanks obtained in degassed H_2SO_4 without ethanol or O_2.

Catalysts	ECSA/m^2 g_{pt}^{-1}	Onset potential for ORR[a]/V	Peak potential of ORR/V	ORR current at 0.53 V ($\times10^{+4}$ A)	H_2O_2 oxidation current at 0.9 V ($\times10^{+5}$ A)	Onset potential for EOR/V	Preferable use: EOR or ORR
Pt/C	20.63	0.658	0.476	−3.75	8.94	0.328	N/A[b]
PtMn/C	22.26	0.641	0.412	−2.75	6.75	0.402	ORR
PtMnFe/C	23.61	0.626	Undefined	−2.66	11.90	0.341	EOR
PtMnCo/C	20.46	0.648	0.518	−3.82	8.87	0.362	ORR
PtMnNi/C	24.79	0.645	Undefined	−2.54	12.01	0.380	ORR
PtMnCu/C	23.15	0.708	0.535	−4.57	12.33	0.284	Both reactions but much better for ORR
PtMnMo/C	20.23	0.631	0.479	−4.21	6.85	0.227	EOR
PtMnSn/C	22.84	0.561	0.277	−0.63	3.21	0.218	EOR
PtMnCuFe/C	17.80	0.674	0.524	−7.73	12.10	0.236	Both reactions but much better for EOR
PtMnCuCo/C	19.82	0.659	0.526	−3.82	11.24	0.272	Both reactions but much better for EOR
PtMnCuNi/C	16.38	0.659	0.515	−8.69	5.93	0.232	Both reactions but much better for EOR
PtMnCuSn/C	19.98	0.658	0.508	−5.09	9.05	0.239	EOR
PtMnMoFe/C	31.26	0.665	0.471	−3.78	10.28	0.167	Both reactions but much better for EOR
PtMnMoCo/C	12.34	0.641	0.407	−2.52	7.44	0.142	EOR
PtMnMoNi/C	23.36	0.663	0.509	−3.5	9.17	0.148	Both reactions but much better for EOR
PtMnMoCu/C	18.57	0.680	0.528	−8.68	16.33	0.224	Both reactions but much better for EOR
PtMnMoSn/C	11.98	0.648	0.449	−2.61	8.79	0.059	EOR

[a] All potentials reported here are with respect to the Ag/AgCl reference electrode.
[b] taken as reference to evaluate the other catalysts for EOR and ORR.

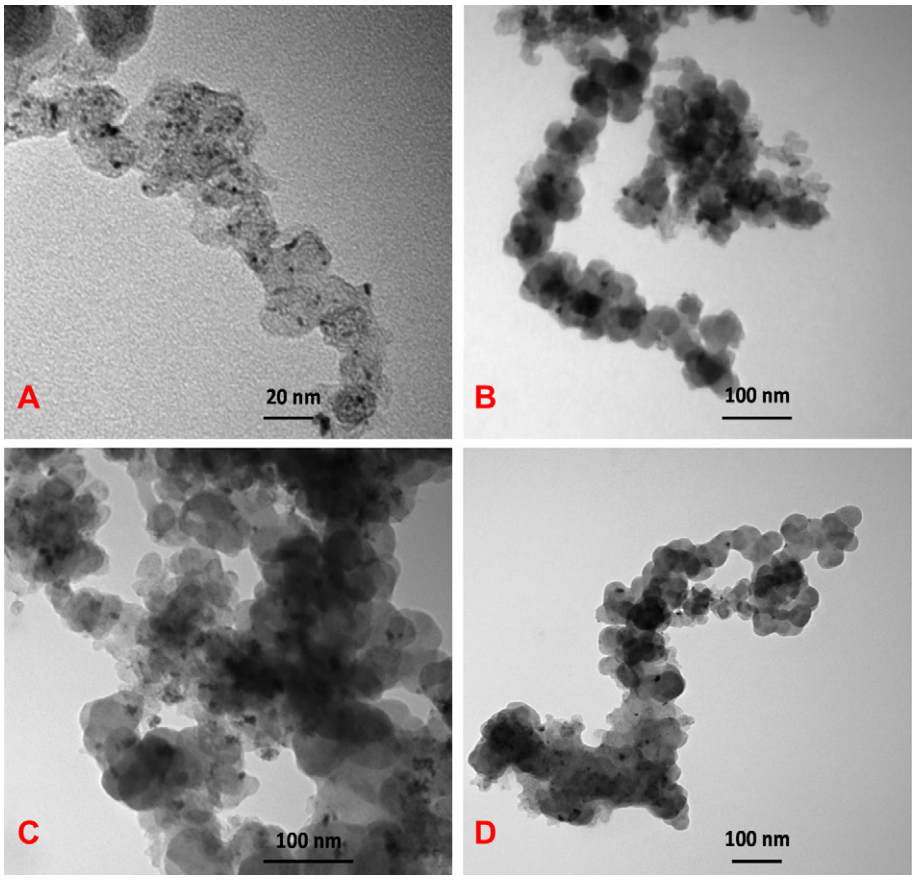

Fig. 2. TEM images of PtMnCu/C (A), PtMnSn/C (B), PtMnCuFe/C (C) and PtMnCuSn/C (D).

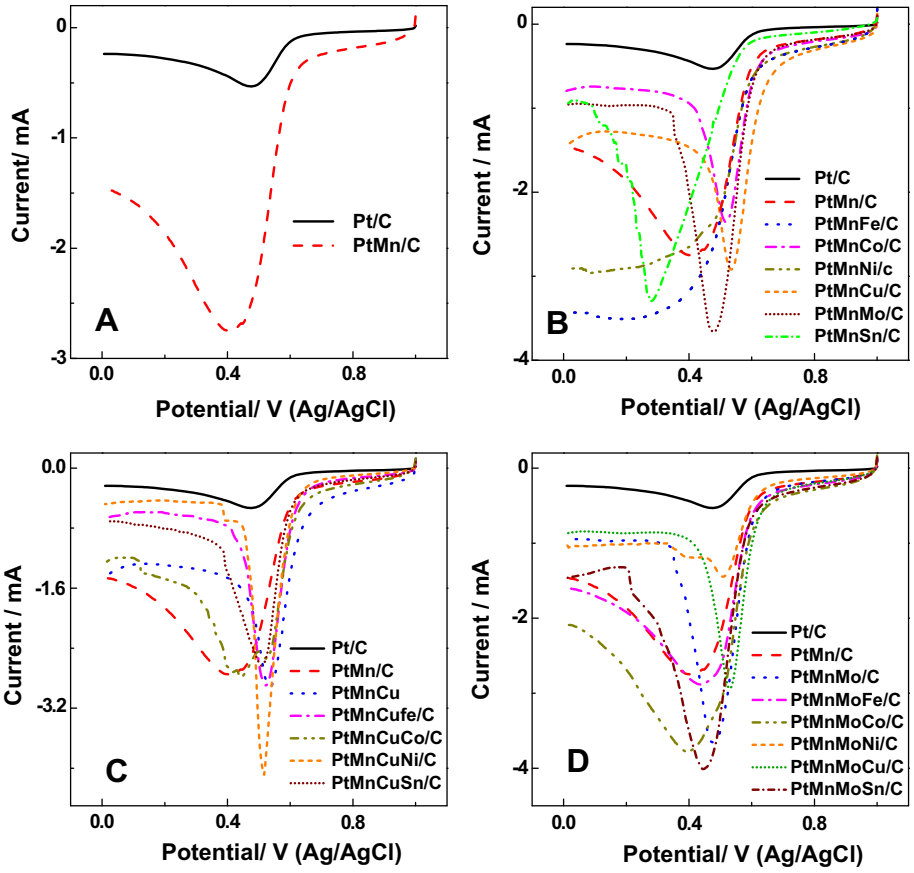

Fig. 3. Is Fig. 1 normalized per milligram of Pt determined by ICP (Table 1).

molecule following pathway k_1 (Eo = 0.69 and 1.23 V vs. NHE, respectively) [39]. On the other hand, if the produced H_2O_2 is further transformed into H_2O following the rate k_3, the overall reaction to reduce O_2 into H_2O passing through H_2O_2 will require more energy (Eo (k_3) = 1.76 V vs. NHE) [39].

From the application standpoint, for an efficient operation of a cathode of fuel cells, a number of conditions must be satisfied. Among the important ones is that the redox potential of the cathode where O_2 is reduced should be as positive as possible to give the maximum potential difference between the anode and cathode. Another prerequisite for an efficient fuel cells cathode is that the current intensity of the ORR induced for the same O_2 concentration for all catalysts (comparative study for the saturated O_2 solution) has to be as high as possible because high current reflects a fast reaction [8,39].

Thus, onset potential ((I) in Fig. 1A) and current intensity and sharpness of the peaks ((II) in Fig. 1A) are the two main criteria used in this study to identify the best catalysts for the ORR among the synthetized binary PtMn/C, ternary PtMnX/C (X = Fe, Co, Ni, Cu, Mo and, Sn) and quaternary PtMnCuX/C (X = Fe, Co, Ni, and Sn) and PtMnMoX/C (X = Fe, Co, Ni, Cu and Sn) alloy catalysts [8,39]. The advantage of this method is the simplicity and the accuracy at the condition that the experiments are well done in a comparative manner, which the case of the present study. All the results are compared with respect to pure Pt/C synthetized under the same conditions. The other criteria which may qualitatively help to identify the presence of issued H_2O_2 from the ORR in cyclic voltammetry is the oxidation current ((III) in Fig. 1A) observed upon reverse scan of O_2 reduction. Because H_2O_2 is easily oxidized at Pt and Pt alloys, if issued from the ORR, an increase in the oxidation current will follow and the intensity of the oxidation current would be proportional to the amount of the produced H_2O_2. Although, the latter is rarely addressed in literature for fuel cells catalysts, it is important to bear in mind that is the main criteria used in biosensors based H_2O_2 detection [40–43].

3.2. Activity of binary PtMn/C, ternary PtMnX/C (X = Fe, Co, Ni, Cu, Mo and, Sn) and quaternary PtMnCuX/C (X = Fe, Co, Ni, and Sn) and PtMnMoX/C (X = Fe, Co, Ni, Cu and Sn) alloy catalysts towards ORR

Fig. 1 illustrates the response of binary PtMn/C, ternary PtMnX/C (X = Fe, Co, Ni, Cu, Mo and, Sn) and quaternary PtMnCuX/C (X = Fe, Co, Ni, and Sn) and PtMnMoX/C (X = Fe, Co, Ni, Cu and Sn) alloys catalysts towards the reduction of O_2 with respect to pure Pt/C. The values of the electrochemical active surface area (ECSA), onset potential, peak potential, reduction current intensity of the ORR and, oxidation current intensity of the issued H_2O_2 are compiled in Table 2. Fig. 1 displays that only some catalysts show improved activity towards the reduction of O_2 in terms of onset potential if compared to Pt/C. The latter is different from what has been observed previously with ethanol, where most binary, ternary and quaternary catalysts revealed enhanced activities towards ethanol oxidation if compared to Pt/C [26–28].

In the group of binary alloys, Fig. 1A and Table 2 depict that PtMn/C has slightly less activity than Pt/C towards O_2 reduction because the onset potential of the ORR is slightly less positive. Also the current intensity of the ORR is lower for PtMn/C compared to Pt/C. Consequently, the oxidation current intensity of the issued H_2O_2 is also lower for PtMn/C compared to Pt/C. The latter is understandable because the amount of the H_2O_2 produced from ORR

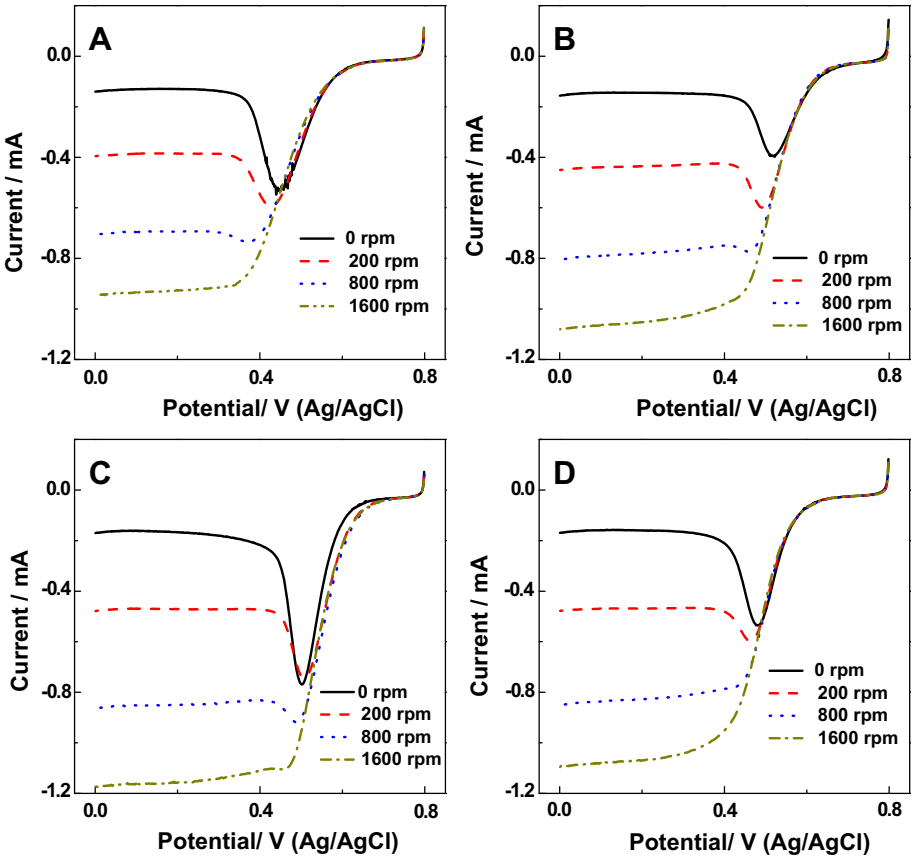

Fig. 4. Pt/C (A), PtMnCu/C (B), PtMnCuFe/C (C) and PtMnMoCu/C (D) catalysts in 0.5 M H_2SO_4 saturated with O_2 at 0, 200, 800 and 1600 rpm. Scan rate 20 mV s^{-1}.

is proportional to the current intensity of the ORR. In other words, the less H_2O_2 is produced, the less it is oxidized. Harlow et al. [44] recently reported PtMn catalysts prepared by sputtering with improved ORR activity that is mainly due to the dissolution of Mn-oxides creating a rougher Pt surface for ORR. Since our catalysts are primarily based on the alloy phase (with only a small portion of oxide) [27,28], this suggests that the Pt–Mn alloy phase is less active towards the ORR.

In the group of ternary alloys, PtMnCu/C looks promising for the ORR. With more than 50 mV gain in potential, the ORR is energetically facilitated with PtMnCu/C compared to pure Pt/C and PtMn/C. Also, high current intensities and sharper peak can be noticed with PtMnCu/C, reflecting fast kinetics of the ORR. High oxidation currents can also be observed in Fig. 1B and Table 2 with PtMnCu/C. This suggests generation of high amount of H_2O_2 from the ORR. In this group of ternary alloys, Fig. 1B depicts cyclic voltammograms with different shapes and forms. This reflects different ORR pathways with the ternary alloys catalysts. Although, it is complicated to identify the detailed pathways of the ORR, onset potential ((I) in Fig. 1A) and oxidation current ((III) in Fig. 1A) may yield some information. For example, while the onset potential of ORR with PtMnFe/C, PtMnCo/C, PtMnNi/C and PtMnMo/C are located in same region as Pt/C, the onset potential of ORR with PtMnSn/C is shifted by 97 mV towards less positive potentials. This suggests that the ORR with PtMnSn/C is energetically less favorable. On the other hand, analysis of the cyclic voltammetry curve of PtMnSn/C in the oxidation region ((III) in Fig. 1A) of which the current value is proportional to the amount of the generated H_2O_2, Fig. 1B and Table 2 reveal the lowest value. This means that the pathway or mechanism of ORR with PtMnSn/C is different from Pt/C and the other ternary catalysts. The absence of significant amounts of H_2O_2 suggests that the ORR at PtMnSn/C yields mainly H_2O as final product which cannot be oxidized and yield significant oxidation current. The latter may occur with a two steps pathway of which the first produces H_2O_2 with $2e^-$ reaction and then in turn H_2O_2 reduced into H_2O (pathways k_2 and k_3 in Scheme 1) or, O_2 is directly reduced into H_2O with a $4e^-$ reaction (pathway k_1 in Scheme 1). Since the onset potential of ORR with PtMnSn/C is significantly sifted towards less positive potentials, one may suggest that the second pathway took place because, thermodynamically, it requires more overpotential (Eo = 1.23 V vs. NHE) than the first proposed pathway (Eo = 0.69 V vs. NHE) [39]. On the other hand, we can rule out the possibility that PtMnSn/C does not efficiently catalyze the oxidation of H_2O_2 because our results showed that the activity of PtMnSn/C towards the oxidation of H_2O_2 is close to the activity of the other catalysts (data not shown). Therefore, it can be concluded that while with most of the ternary catalysts, the pathway that generates a portion of H_2O_2 as a final product occur; the ORR with PtMnSn/C produces mainly H_2O as a final product. ECSAs and grain size are usually parameters that help to evaluate the catalytic performances of catalysts. As can be seen in Table 2, ECSAs of the ternary alloys series are pretty close and PtMnCu/C do not show the highest ECSA of the this group of catalysts in order to explain its high efficiency towards ORR. However, the grain sizes look different from one catalyst to another. For example, PtMnSn/C has the largest grain size with two different phases and PtMnCu/C displays the smallest grain size. The latter may have an impact on the ORR mechanism. On the other hand, nature of the catalyst and combination between the different metals to form the alloys may be the primary reason that promotes or not the ORR.

In the group of quaternary alloys, many of the catalysts display sharper peaks indicating fast kinetics and among the catalysts

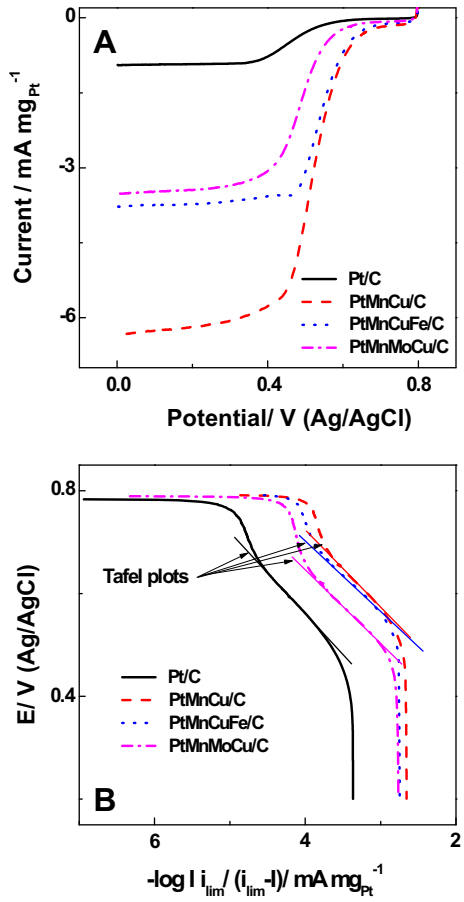

Fig. 5. (A) Comparison between the cyclic voltammetry curves of Pt/C, PtMnCu/C, PtMnCuFe/C and PtMnMoCu/C normalized per milligram of Pt in 0.5 M H_2SO_4 saturated with O_2 at 1600 rpm. (B) E versus $-\log I\, i_{lim}/(i_{lim} - I)$, showing the Tafel plots in the linear zone of each curve.

PtMnCuFe/C looks very promising for the ORR. With a gain in potential of 16 mV compared to pure Pt and an increase in current intensity of the ORR by almost 2 folds, PtMnCuFe/C shows better activity towards the ORR compared to pure Pt/C. In this group, PtMnCuNi/C displays close onset potential with respect to Pt/C and superior catalytic current, suggesting that PtMnCuNi/C is more active than Pt/C. On the other hand, while PtMnSn/C recorded the lowest activity towards ORR, the quaternary alloy PtMnCuSn/C looks slightly better than Pt/C especially in terms of current intensity of the ORR. Smaller grain sizes as well as better dispersion of the catalyst on the supporting carbon may be one reason for the enhanced activity [24]. As depicted in TEM images of Fig. 2, while PtMnSn/C shows agglomerations, PtMnCuSn/C displays a better distribution and smaller grain sizes similar to PtMnCu/C and PtMnCuFe/C, which illustrated high activities towards ORR. With respect to ECSAs, Table 2 illustrates that the group of quaternary alloys have slightly smaller ECSAs compared to the ternary alloys, which cannot explain the improvement of the catalysis of ORR. In addition, in this group, no correlation between ECSAs and superior activity can be noticed. This leads us to the conclusion that the primary reason for the activity of the catalysts towards the ORR may have to do with the composition of the alloy, which may promote or not the ORR.

In the last group of PtMnMo/C based quaternary alloys, PtMnMoCu/C looks also very promising for the ORR and eventually for use in cathodes of fuel cells. With a gain in potential of 22 mV and an increase in the current intensity of the ORR by almost two folds, PtMnMoCu/C seems to have a relevant catalytic activity towards the ORR with respect to Pt/C, PtMn/C and PtMnMo/C precursors. Careful analysis of Fig. 1D and Table 2 reveals that PtMnMoCu/C shows the highest value of oxidation current. This indicates that large amounts of H_2O_2 are produced from the ORR as a final product. On the other hand, the other catalysts of this group seem to have either a close activity to that of Pt/C such as PtMnMoFe/C and PtMnMoNi/C or slightly less active like PtMnMoCo/C and PtMnMoSn/C. Analysis of the grain size of this group of catalysts shown in Table 1 depicts that they are slightly higher than the quaternary group based PtMnCu/C, and PtMnMoCu/C have the smallest grain size. The latter may contribute to its efficiency towards the ORR. On the other hand, ECSA of PtMnMoCu/C is below that of Pt/C, PtMn/C and PtMnMo/C, hence cannot explain its enhanced catalytic activity. As a result, we also concur with the conclusion that the primary reason for the activity of the some catalysts towards the ORR is the composition of the alloys with some contribution from the grain size and distribution of the catalysts on the supporting carbon.

Although Fig. 1 demonstrates that only some catalysts are promising for the ORR, when normalized per milligram of Pt, all catalysts look more active than Pt/C (Fig. 3). However, it is important to bear in mind that from the application standpoint for fuel cell devices, the results of Fig. 1 are more realistic than those shown in Fig. 3. However, Fig. 3 clearly points to the cost benefit of the various Pt alloys catalysts compared to Pt/C. In other words, if Pt alloys display close activities towards the ORR compared to Pt, it is cheaper to use Pt alloys rather than Pt/C because the price will be divided by a factor of 3–8 for these series of the synthetized catalysts (see alloy composition in Table 1).

3.3. Hydrodynamic measurements

In order to have a better idea on the ORR, some of the best catalysts identified by cyclic voltammetry in quiescent conditions were selected for further study by RDE and RRDE. We have selected the best representative catalyst for the series of ternary and quaternary alloys based Cu and Mo. For binary alloys, since PtMn/C did not show significant improvement towards the ORR with respect to Pt/C, no further studies has been done with this catalyst. Fig. 4 displays how the ORR linear sweep voltammogram of Pt/C, and best catalyst of each group of ternary PtMnCu/C and quaternary PtMnCuFe/C and PtMnMoCu/C alloys vary with rotation speed. It can be seen that all the voltammograms display an initial redox wave characteristic of the ORR followed by a limiting current plateau, characteristic of a mass transfer limiting process [39]. For all catalysts, there is an increase in the current response of the ORR as well as the limiting current plateau with the rotation speed and at 1600 rpm, the process seems to be purely diffusion limited [39]. The latter is understandable because the convection effect is so intense at 1600 rpm that the reduction process is governed by mass transport. Two components can be extracted from Fig. 4: i)

Table 3
Summary of the most active catalysts towards ORR, estimate of the Tafel plots determined from Fig. 5B, the average number of the electrons transferred during the reduction process of O_2 determined from Fig. 6A, values of i_k determined from Fig. 6A and H_2O_2% estimated at +0.3 V from Fig. 6B.

Catalyst	Tafel slope (mV dec^{-1})	Number of the electrons transferred (n)	i_k (mA)	H_2O_2% (at 0.3 V vs. Ag/AgCl)
Pt/C	70	3.57	3.89	1.71
PtMnCu/C	67	3.74	4.11	3.78
PtMnCuFe/C	62	3.84	6.28	4.06
PtMnMoCu/C	61	3.95	3.99	5.64

variation of overpotential with current, so called Tafel plots and, ii) variation of reverse current with reverse square root of rotation speed, so called Koutecky–Levich relationship. Each of these components will be analyzed in order to gain a better understanding of the ORR with these selected best catalysts.

3.3.1. Tafel plots

Fig. 5B shows the mass transport corrected Tafel plots of E versus $\log I\, i_{lim}/(i_{lim} - I)$ corrected Pt mass for Pt/C, PtMnCu/C, PtMnCuFe/C and PtMnMoCu/C. i_{lim} represents the limiting current determined by the current plateau for each catalyst. Since the overpotential looks large, we assume that the backward reaction is negligible and the current, I, can be written as [45]:

$$I = i^{\circ} e^{\frac{n\alpha FE}{RT}} \quad (2)$$

where i^o is the exchange current, n is the number of the electron transferred, α is the transfer coefficient and F, R and T have their usual meaning.

The slope of $\log I$ versus E is called Tafel slope and since all other parameters in the Tafel slope are known, the only parameters determining the Tafel slope are the overpotential E and $n\alpha$. It is worth reminding that the higher the Tafel slope is, the faster the overpotential increase with the current intensity [45]. Thus, in order to obtain a high current at low overpotential, an electrochemical reaction should exhibit a low Tafel slope or a large $n\alpha$. For the ORR, the Tafel slopes are usually close either to 60 mV dec^{-1} if an average 2e$^-$ is exchanged or 120 mV dec^{-1} if an average of 1e$^-$ process took place [45]. The estimated Tafel slopes from Fig. 5B are summarized in Table 3. It can be seen that the Tafel slopes are close to 60 mV dec^{-1}, meaning 2e$^-$ transfer process probably took place during the ORR. The Tafel slopes are close to the values determined in literature for other Pt and Pt alloys catalysts including PtCo, PtCu, PtNi and, PtRhFe [6,46,47]. The values of Table 3 are consistent with the results of cyclic voltammetry of Fig. 1 and Table 2 discussed in the previous section which illustrate the presence of H_2O_2 as final product of ORR. Also, Tafel plots of the catalysts normalized per mg of Pt display that activity of the catalysts decreases in the following order: PtMnMoCu/C > PtMnCuFe/C > PtMnCu/C > Pt/C. The difference in Tafel slopes can be explained by the change in the adsorption behavior of the oxide species with the promoting metal co-catalysts atoms on the particle surface [6].

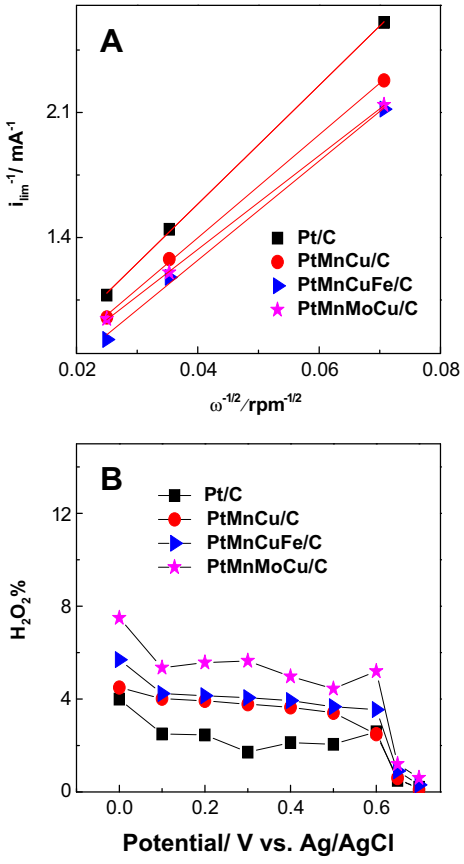

Fig. 6. (A) Linear relationship between $1/i_{lim}$ at −0.2 V vs. Ag/AgCl versus $1/\omega^{1/2}$ taken from Fig. 4 for Pt/C, PtMnCu/C, PtMnCuFe/C and PtMnMoCu/C. (B) Variation of H_2O_2% estimated using Eq. (1) with the disk potential at speed of 800 rpm.

3.3.2. Koutecky–Levich

Fig. 6A shows the variation of reverse of the limiting current, $1/i_{lim}$ estimated at −0.2 V vs. Ag/AgCl versus reverse of the square root of rotation speed, $1/\omega^{1/2}$. A linear relationship can be noticed between the two parameters, meaning that the kinetics of the ORR can be analyzed by means of Koutecky–Levich equation [39]:

$$\frac{1}{i_{lim}} = \frac{1}{i_k} + \frac{1}{0.62nFAD^{2/3}\nu^{1/6}C\omega^{1/2}} \quad (3)$$

where i_k represents the current in absence of any-mass transfer effects, n is the number of the electron transferred, F is the Faradaic number (96,500 C mol^{-1}), A is the area of the electrode in cm^2 (0.1962 cm^2), C is the concentration of O_2 in the bulk solution (0.25 mM), D is the diffusion coefficient of O_2 (2.2×10^{-5} cm^2 s^{-1}) and ν is the kinematic viscosity of water (0.01 cm^2 s^{-1}).

The estimated values of n for Pt/C, PtMnCu/C, PtMnCuFe/C and PtMnMoCu/C are compiled in Table 3. It can clearly be seen that the average number of the electrons involved in the ORR process are close to 4e$^-$. This suggests that the pathways with rate constants k_2 and k_3 of Scheme 1 surely took place to produce H_2O_2 and H_2O as final products. Table 3 also depicts that the average number of the electrons involved in the reduction process of O_2 decreases in the following order: PtMnMoCu/C > PtMnCuFe/C > PtMnCu/C > Pt/C. All these data support the results from cyclic voltammetry and Tafel plots, which suggest that PtMnMoCu/C is the most active catalyst for ORR followed by PtMnCuFe/C, PtMnCu/C and Pt/C. In terms of kinetic of the ORR, Table 3 also reveals that i_k values of the alloys are relatively higher with respect to Pt/C, meaning that the kinetics of the ORR is fast with the alloy catalysts.

3.3.3. Estimation of the H_2O_2%

In order to have a better idea of the reaction products issued from the ORR (H_2O, H_2O_2 or a mixture of both), the amount of the generated H_2O_2 was quantitatively evaluated with RRDE as a function of the applied potential and the results are shown in Fig. 6B. It will be noted that the established H_2O_2 for all catalysts ranges from 0.2% to 7.5%. Also, the amount of H_2O_2 increases in the beginning of polarization at high overpotentials, passes by a stabilization at intermediates potentials then increases again at less positive potentials. The highest H_2O_2 concentration was detected at potential of 0 V vs. Ag/AgCl due probably to presence of high amount of co-adsorbed deposited H_2O_2 molecules. Also, it can be seen that Pt/C generates the least H_2O_2. PtMnCu/C and PtMnCuFe/C show close quantities and the highest H_2O_2% is produced with PtMnMoCu/C. The latter is consistent with the results of cyclic voltammetry and RDE.

Although at this stage the reasons and the mechanisms are not fully understood, nevertheless, due to the low H_2O_2% (<7.5%) and the high number of the exchanged electrons during the reduction process (close to 4e$^-$ for all the catalysts), one may suggest that different

pathways took place during the ORR. Since all data points to presence of H_2O_2 as final product, O_2 is surely reduced following the pathways with rate constants k_2 and k_5 to produce adsorbed H_2O_2 which will then be desorbed to leave the catalyst surface towards the solution. With respect to this, k_2 and k_5 play very important roles in the estimated H_2O_2%. Because the estimated H_2O_2% is greater with the alloys (PtMnMoCu > PtMnCuFe > PtMnCu) compared to Pt, one can suggest that k_2 of alloys in the respective orders are greater than that of Pt. On the other hand, k_5 depends on nature of the catalyst and its activation energy (E_a) of desorption of H_2O_2 molecules from the catalyst surface [48]. Accordingly, the results of H_2O_2% listed in Table 3 may indicate that E_a (PtMnMoCu) < E_a (PtMnCuFe) < E_a (PtMnCu) < E_a (Pt). This means that the alloys have superior catalytic performance towards the desorption of adsorbed H_2O_2 molecules on the catalyst surface than Pt. However, at this stage it is quite difficult to argue which of k_2 or k_5 is dominant in the estimated H_2O_2%. Other pathways following the rate constant k_3 to reduce big part of the generated H_2O_2 into H_2O also took place because the estimated H_2O_2% is relatively low (<7.5%), meaning that big part of the reaction products is H_2O. Finally, the scenario of reduction of O_2 with a $4e^-$ reaction following rate constant k_1 may also be possible in combination with previously described pathways.

3.4. Preferable use of the catalysts at anode or cathode of fuel cells (ethanol/O_2)

In order to have a better idea on the preferable use of the synthetized catalysts either at anode or cathode of fuel cells (ethanol/O_2), we have compared their onset potentials towards the oxygen reduction reaction (ORR) versus ethanol oxidation reaction (EOR) with respect to pure Pt/C taken as a reference supposing that Pt/C is good for both reactions ORR and EOR. The last column of Table 2 shows the preferable use of each catalyst. It will be noted that although most catalysts can be used for both reactions to promote the catalysis of the fuel (ethanol or O_2), some of them are better for use at the anode and others at the cathode. The goal of this comparison is to identify the best catalysts that might be incorporated in fuel cells cathodes and anodes to yield fuel cells with appreciable output voltages. It can be seen that from this series of alloys catalysts, it is possible to construct fuel cells with relevant selectivities to both reactions. Among the best combinations to consider for fuel cells applications that yield large operating voltages (anode catalyst (EOR)/cathode catalyst (ORR)) are: PtMnMoSn/PtMnCu, PtMnMoNi/PtMnCu, PtMnMoCo/PtMnCu, and PtMnMoFe/PtMnCu. Other combinations but with lower outputs voltages are also possible (Table 2).

4. Conclusions

In this account, we have evaluated the activity of binary PtMn/C, ternary PtMnX/C (X = Fe, Co, Ni, Cu, Mo and, Sn) and quaternary PtMnCuX/C (X = Fe, Co, Ni, and Sn) and PtMnMoX/C (X = Fe, Co, Ni, Cu and Sn) alloys catalysts towards the oxygen reduction reaction (ORR) in acidic solution. Although all catalysts exhibited improved activities towards the ORR if normalized per mg of Pt under the same conditions of saturated O_2 solution, when the catalysts were considered per milligram of total metal; only some of them illustrated improved activities towards the ORR in terms of onset potential and current intensity determined by cyclic voltammetry with respect to pure Pt/C. PtMnCu/C, PtMnCuFe/C and PtMnMoCu/C were found to be the best catalysts for ORR. In order to gain better understanding of the pathways of ORR, Pt/C. PtMnCu/C, PtMnCuFe/C and PtMnMoCu/C were further studied by rotating disk electrode and rotating ring disk electrode. Tafel plots and Koutecky–Levich analysis of the data revealed that the activity towards the ORR is better with PtMnMoCu/C followed by PtMnCuFe/C and PtMnCu/C. The estimated average number of the electrons transferred during the ORR process was found to be around $4e^-$. The average percentage of the generated H_2O_2 reached as high as ~7.5% with PtMnMoCu/C. All these data point to the fact that the pathways of ORR that produce H_2O_2 and H_2O as final products took place. As a final comparison for this series of catalysts, this study also gives a better selection of the catalysts that may preferably be used at the anode for ethanol oxidation or at the cathode for ORR to yield fuel cells with substantial outputs voltages.

Acknowledgement

This work was supported by Alcohol Countermeasure Systems Corp., the Natural Sciences and Engineering Research Council (NSERC) of Canada and UOIT. We thank Wen He Gong (McMaster University) for the XRD data, Michael Allison (UOIT) for assistance with the ICP measurements and Dr. Richard B. Gardiner (University of Western Ontario) for the TEM images.

References

[1] A.S. Arico, S. Srinivasan, V. Antonucci, Fuel Cells 1 (2001) 133.
[2] K. Kordesch, G. Simader, Fuel Cells and Their Applications, VCH, Weinheim, 1996.
[3] J.K. Nørskov, J. Rossmeisl, A. Logadottir, L. Lindqvist, Journal of Physical Chemistry B 108 (2004) 17886.
[4] H. Tang, Z. Qi, M. Ramani, J.F. Elter, Journal of Power Sources 158 (2006) 1306.
[5] C.H. Brian, A. Heinzel, Nature 414 (2001) 345.
[6] M. Oezaslan, F. Hasche, P. Strasser, Journal of the Electrochemical Society 159 (2012) B444.
[7] Y. Kiros, International Journal of Electrochemical Sciences 2 (2007) 285.
[8] M. Ammam, B. Keita, L. Nadjo, I.M. Mbomekalle, M.D. Ritorto, T.M. Anderson, W.A. Neiwert, C.L. Hill, J. Fransaer, Electroanalysis 23 (2011) 1427.
[9] M. Ammam, I.M. Mbomekalle, B. Keita, L. Nadjo, T.M. Anderson, X. Zhang, K.I. Hardcastle, C.L. Hill, J. Fransaer, Journal of Electroanalytical Chemistry 647 (2010) 97.
[10] D. Zhang, D. Chi, T. Okajima, T. Ohsaka, Electrochimica Acta 52 (2007) 5400.
[11] S. Gottesfeld, T.A. Zawodzinski, Polymer electrolyte fuel cells, in: Advances in Electrochemical Science and Engineering, vol. 5, Wiley-VCH, Weinheim, 1997.
[12] J. Zhao, A. Manthiram, Applied Catalysis B: Environmental 101 (2011) 660.
[13] S. Mukerjee, S. Srinivasan, M.P. Soriaga, Journal of Physical Chemistry 99 (1995) 4577.
[14] P. Mani, R. Srivastava, P. Strasser, Journal of Power Sources 196 (2011) 666.
[15] G. Tamizhmani, G.A. Capuano, Journal of the Electrochemical Society 141 (1994) 968.
[16] F. Godinez-Salomon, J.M.H. Lopez, O. Solorza-Feria, ECS Transactions 36 (2011) 541–548, 1, MES 26: Electrochemistry as a Tool for Sustainable Development.
[17] C. Guelduer, S. Guenes, Catalysis Communications 12 (2011) 707.
[18] S.J. Hwang, S.J. Yoo, S. Jang, T.H. Lim, S.A. Hong, S.K. Kim, Journal of Physical Chemistry C 115 (2011) 2483.
[19] Y. Ma, P.B. Balbuena, Journal of the Electrochemical Society 157 (2010) B959.
[20] E. Kreidler, T. He, in: He Ting (Ed.), Catalysts for Oxygen Electroreduction (2009), pp. 63–90.
[21] F.J. Luczak, D.A. Landsman, Ordered Ternary Fuel Cell Catalysts Containing Platinum and Cobalt (1987). US-Patent No. 4711 829.
[22] F.J. Luczak, D.A. Landsman, Ternary Fuel Cell Catalysts Containing Platinum, Cobalt and Chromium (1984). US-Patent No. 4447 506.
[23] F.J. Luczak, D.A. Landsman, Ordered Ternary Fuel Cell Catalysts Containing Platinum and Cobalt and Method for Making the Catalysts (1987). US-Patent No. 4 677 092.
[24] B.C. Beard, P.N. Ross Jr., Journal of the Electrochemical Society 137 (1990) 3368.
[25] J.T. Glass, G.L. Cahen, G.E. Stoner, E.J. Taylor, Journal of the Electrochemical Society 134 (1987) 58.
[26] M. Ammam, L.E. Prest, A.D. Pauric, E.B. Easton, Journal of the Electrochemical Society 159 (2012) B195.
[27] M. Ammam, E.B. Easton, Journal of the Electrochemical Society 159 (2012) B635.
[28] M. Ammam, E.B. Easton, Journal of Power Sources 215 (2012) 188.
[29] O. Antoine, R. Durand, Journal of Applied Electrochemistry 30 (2000) 839.
[30] U.A. Paulus, T.J. Schmidt, H.A. Gasteiger, R.J. Behm, Journal of Electroanalytical Chemistry 495 (2001) 134.
[31] C. Medard, M. Lefevre, J.P. Dodelet, F. Jaouen, G. Lindbergh, Electrochimica Acta 51 (2006) 3202.
[32] A.D. Pauric, A.W. Pedersen, T. Andrusiak, E.B. Easton, Journal of the Electrochemical Society 157 (2010) B370.

[33] K. Kinoshita, Electrochemical Oxygen Technology, John Wiley & Sons, New York, 1992.
[34] H. Wroblowa, Y.C. Pan, J. Razumney, Journal of Electroanalytical Chemistry 69 (1976) 195.
[35] V. Stamenkovic, N.M. Markovic, P.N. Ross Jr., Journal of Electroanalytical Chemistry 500 (2000) 44.
[36] B.N. Grgur, N.M. Markovic, P.N. Ross Jr., Canadian Journal of Chemistry 75 (1997) 1465.
[37] N.M. Markovic, H.A. Gasteiger, B.N. Grgur, P.N. Ross, Journal of Electroanalytical Chemistry 467 (1999) 157.
[38] N.M. Markovic, T.J. Schmidt, V. Stamenkovic, P.N. Ross, Fuel Cells 1 (2001) 105.
[39] A.J. Bard, L.R. Faulkner, Electrochemical Methods: Fundamentals and Applications, second ed., Wiley, NY, 2001.
[40] M. Ammam, J. Fransaer, Biosensors and Bioelectronics 25 (2010) 1597.
[41] M. Ammam, E.B. Easton, Sensors and Actuators B: Chemical 155 (2011) 340.
[42] G.S. Wilson, M. Ammam, FEBS Journal 274 (2007) 5452.
[43] J. Wang, Chemical Reviews 108 (2008) 814.
[44] J.E. Harlow, D.A. Stevens, R.J. Sanderson, G.C.-K. Liu, L.B. Lohstreter, G.D. Vernstrom, R.T. Atanasoski, M.K. Debe, J.R. Dahn, Journal of the Electrochemical Society 159 (2012) B670.
[45] C. Song, J. Zhang, in: J. Zhang (Ed.), PEM Fuel Electrocatalysts and Catalyst Layers: Fundamental and Applications, Springer, 2008.
[46] M. Oezaslan, P. Strasser, Journal of Power Sources 196 (2011) 5240.
[47] U.A. Paulus, A. Wokaun, G.G. Scherer, T.J. Schmidt, V. Stamenkovic, N.M. Markovic, P.N. Ross, Electrochimica Acta 47 (2002) 3787.
[48] G.A. Somorjai, Y. Li, Introduction to Surface Chemistry and Catalysis, John Wiley and Sons, 2010. [Section 4.6].